RSC Advances

ROYAL SOCIETY OF CHEMISTRY

www.rsc.org/advances

ARTICLE TYPE www. rsc.org/xxxxxx | XXXXXXXX

Electron transport enhanced by electrode surface reconstruction: A case study of C_{60}-based molecular junctions

Q. Q. Wu,[a,b] X. H. Zheng,[b] X. Q. Shi,[,c,b,*] J. Lan, [b]H. Hao [b]and Z. Zeng[b,d,‡]

Received Xth XXXXXXXXXX 20XX, Accepted Xth XXXXXXXXX 20XX
First published on the web Xth XXXXXXXXXX 200X
DOI: 10.1039/b000000x

The effects of surface reconstruction on electron transport of two monolayers of C_{60} sandwiched between two Cu(111) bulk electrodes have been investigated by density functional theory (DFT) calculations combined with a nonequilibrium Green's function technique. Two markedly different electrode surface structures have been considered, which have been obtained in previous experimental works: one with an unreconstructed perfect surface and the other with a surface reconstruction with a 7-atom-missing hole per (4×4) Cu(111) cell. The results indicate that surface reconstruction induces an increase of more than 50% in the current at low bias. Molecular-orbital projected density of states (MO-PDOS) analysis reveals that the change in transport properties originates from the enhanced orbital-dependent electrode-molecule coupling and the increased charge transfer from electrodes to molecules. Our current work suggests that surface reconstruction could play a very important role in the electron transport properties; and hence surface reconstruction (or more generally realistic atomic contact details) should be taken into full consideration in the simulation and design of molecular devices, especially when it is expected to reproduce computationally the experimental observations.

1 Introduction

Molecular junctions composed of individual or monolayer of molecules sandwiched between two conducting electrodes have been the focus of both theoretical and experimental scientists over the past decades.[1–3] Due to the rich interesting transport behaviors that have been observed, such as negative differential resistance (NDR),[4–6] current rectification and amplification,[7,8] electrical switching,[9–11] spin filtering,[12] magnetoresistance,[13] and so on, such devices are expected to be promising alternatives to traditional silicon-based components in the future integrated electronic circuits. However, for real applications of molecular devices, there are still many fundamental issues that have to be resolved. One of the most important problems is the full understanding of the electrode-molecule contact details at the atomic-scale. On one hand, experimentally, in many situations, the electrode-molecule contact details may be dominant in determining the electron transport behaviors in molecular devices.[2,14] Hipps *et al.* even claimed that the investigation of electron transport is all about contacts.[15] On the other hand, theoretically, density functional theory combined with nonequilibrium Green's function has proven to be a very powerful technique for the study of molecular devices at the atomic-scale. However, large discrepancies are observed between the magnitudes of electric current and conductance of theoretical results and the experimental ones.[16–19] One important reason is that the electrode-molecule contact details were not fully considered since all the simulated structures were based on hypothesized ones and probably far from the experimentally measured ones. Consequently, it is critical to take into consideration the interface atomic details as much as we can in molecular electronics simulations.

As a matter of fact, great attention has been paid to this problem. For example, to obtain a robust electrode-molecule coupling, some special anchoring groups are used to serve as linkers between the metallic electrodes and the sandwiched molecules, such as thiol groups, amine groups, and C_{60} molecules.[20–22] In addition, it is well known that charge transfer between the electrodes and molecules is a very important factor in the transport mechanisms of molecular devices and it is suggested that it can be tuned by controlling the number or type of chemical bonds at the molecule/electrode interface. For example, Schull and coworkers demonstrated that the charge injection efficiency varies with the atomic contact details between the scanning tunneling microscope (STM) tip and the C_{60} molecule: the charge injection efficiency at a con-

[a] *School of Physics and Material Science, Anhui University, Hefei 230601, China*
[b] *Key Laboratory of Materials Physics, Institute of Solid State Physics, Chinese Academy of Sciences, Hefei 230031, China*
[c] *Department of Physics, South University of Science and Technology of China, Shenzhen 518055, China*
[d] *Department of Physics, University of Science and Technology of China, Hefei 230026, China*
[*] *Email: shi.xq@sustc.edu.cn; Tel: +86-755-88018206; Fax: +86-755-88018206*
[‡] *Email: zzeng@theory.issp.ac.cn; Tel: +86-551-65591407; Fax: +86-551-65591434*

tact with C=C double bond(6:6 bond) is higher than that with C-C single bond (5:6 bond) and that the lowest charge injection efficiency is presented at a contact with a single C atom .[23] In another STM experiment, the conductance is modulated in a very large range by increasing the number of metal atoms (from one to five) composing the metallic tip in contact with the C_{60} molecule.[24]

Over the past years, the discovery of superconductivity in metal-doped fullerene has spurred intense surveys on structural and electronic properties of highly symmetric C_{60} molecule adsorbed on noble metal surface, the electron transport and thermopower properties of C_{60} molecules sandwiched between metallic electrodes both theoretically and experimentally.[25–34] Interestingly, it is reported that C_{60} molecules adsorbed on Cu(111) surfaces can induce surface reconstruction, *i.e.*, with 7 of 16 Cu atoms missing per 4×4 cell, thus a pit is formed and the C_{60} sinks into the pit and bonds with both the top and second layer of Cu; and the electronic properties are influenced dramatically at 300-400 K according to STM observations.[26] Other studies demonstrated that metal surface reconstruction induced by molecule adsorption, such as C_{60}, graphene and thiolate(SCH_3) adsorption, has been frequently observed.[35–38]

As we know, surface reconstruction will unavoidably affect the bonding of molecules to the substrates. Naturally, the transport properties could be also affected, which is, however, still not well understood. Although generally the band structure or density of states obtained with conventional DFT calculations could provide useful information about the conductivity of a material, how they will behave in a device, particularly how large the conductance is and how the I-V characteristics will be quantitatively can never be obtained by a conventional DFT calculation. Especially, the electronic structures may change greatly under finite bias. In certain situations, even two different conducting materials connected together into a device may produce an insulating state, which obviously can not be predicted just by an inspection of the band structure or density of states.[39] Thus, a fully quantitative calculation of the electron transport in a device configuration is quite necessary if we want to know the surface reconstruction effects on the performance of molecular devices accurately.

In this work, the effects of electrode surface reconstruction on the electron transport of the C_{60}s have been investigated, as a typical case study of C_{60}, graphene and thiol adsorption induced metal surface reconstruction, by first principles calculations. The model structures are composed by two C_{60}-monolayers sandwiched between two Cu(111) surfaces as electrodes with or without surface reconstruction. Similar to other C_{60}-based devices, the electron transport around the Fermi level is mediated by the lowest unoccupied molecular orbital (LUMO) of C_{60}, indicating that charge transfer from the electrodes to the molecules is still the central mechanism of the electron transport. However, with or without surface reconstruction, the magnitude of the equilibrium conductance and the current at low bias, the height and position of the LUMO-mediated transmission peak are all distinctly different, suggesting that the Cu(111) surface reconstruction greatly affects the performances of C_{60}-based electronic devices.

2 Computational Details

The device models consist of two C_{60} monolayers sandwiched between two Cu(111) surfaces. The stacking mode of two C_{60} monolayers are taken from the C_{60} molecular solid with fcc structure along the (111) direction. Two layers instead of one layer of C_{60}s are selected in order to avoid direct electron transmission between electrodes. A 4×4 supercell with lattice constants of 10.0 Å$\times$10.0 Å is chosen for the Cu(111) surface in the xy plane (see Figure 1). Interestingly, in this way, exactly a 4×4 Cu(111) supercell holds one C_{60} molecule and the lattice mismatch between the Cu(111) surface and the C_{60} monolayer is negligible. For the unreconstructed case, the C_{60} is adsorbed on Cu(111) surface above the hcp hollow site with a hexagon oriented to the metal surface, while in the case of reconstructed configuration, since a 7-atom vacancy induced by C_{60} adsorption, with 7 atoms missing at the first layer, tends to be developed in the Cu(111) surface, the C_{60} cage just sinks into the 7-atom vacancy and lies at the fcc site of the second layer.[25–27] The relative stability of the unreconstructed and reconstructed configurations has been fully discussed.[27] The definitions of different adsorption sites on Cu(111)(such as hcp and fcc above) can be found in the literature.[25]

Both the unreconstructed and the reconstructed structures are fully relaxed by the Vienna Ab-initio Simulation Package(VASP)[40,41]and the same parameters as used in Reference 30 are adopted. For the structure relaxation, five Cu(111) atomic layers on each side were selected and the distance between the two C_{60} monolayers along the z direction is eventually relaxed to be 1.10Å, which is approximately the same as the value in the bulk C_{60} solid. For the calculations of electron transport, the electrode supercell consists of 6 Cu(111) atomic layers with ABCABC stacking, in a lattice constant of 12.228 Å along the z direction. On the left and right sides of the C_{60} monolayers, besides the layer with missing atoms in the reconstructed case, four and five complete atomic layers with ABCA and BCABC stacking respectively from the electrodes are selected as the buffer layers.

The electronic structure calculations are performed by the SIESTA package[42] and the transport calculations are performed by TranSIESTA.[43] The ion-electron interaction is described by norm-conserving pseudopotentials and the local density approximation(LDA) in the Ceperly-Alder (CA) form is adopted for the exchange-correlation functional. Single-ζ(SZ) for Cu and double-ζ plus polarization(DZP) for C are

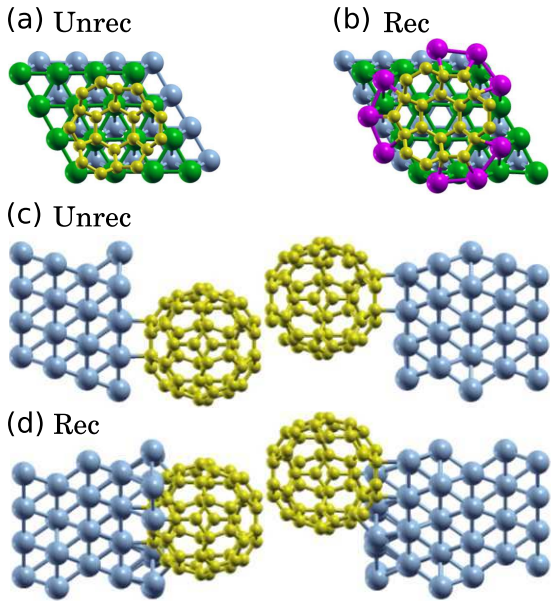

Fig. 1 (color online) The C_{60} molecule on the Cu(111) surface in a 4×4 supercell: (a) at the *hcp* hollow site in the unreconstructed case(abbreviated as "Unrec"); (b) at the *fcc* hollow site in the reconstructed case(abbreviated as "Rec"). In order to see more clearly the bonding features between Cu(111) and C_{60}, only two complete layers of Cu atoms and 21 C atoms closest to the electrode-molecule interface are shown. For contrast, the complete layer closest to C_{60} is shown in green, and the deeper layer in grey. The layer with a 7-atom vacancy (9 atoms remaining) in the reconstructed case is shown in purple. All C atoms are in yellow. (c) and (d) show the scattering region of two-terminal molecular junctions without and with reconstruction. In (c) and (d), all the Cu atoms are in grey.

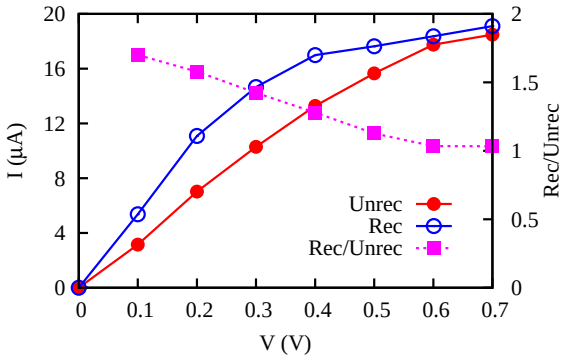

Fig. 2 (color online) Current(I)-voltage(V) curve for the two-terminal devices with unreconstructed and reconstructed electrode surfaces. 'Rec/Unrec' means the current ratio between the two cases.

chosen as the basis set. We choose the basis set this way since it best reproduces the electronic structures (such as density of states and charge transfer) obtained with VASP in the systems concerned in this work. The Brillouin zone for the electrodes is sampled by a $3 \times 3 \times 20$ Monkhorst-Pack grid and that for the scattering region is by $3 \times 3 \times 1$. The choice of a 3×3 k-grid in the xy plane is based on a balance between the accuracy and computation burden and it has been adopted in other literatures for the same size of Cu(111) surface supercells.[25] In order to reduce the computation time in the present study, we have implemented GPU acceleration to speed up the computation of the density matrix which takes up to more than 80% of the total CPU time in the nonequilibrium Green's function scheme and a speed up of 20 times has been achieved with a single Tesla K20 card for a moderate system.[44]

The transmission function at energy E and bias V is calculated through the Landauer formula:[45,46]

$$T(E,V) = Tr[\Gamma_L(E,V)G^R(E,V)\Gamma_R(E,V)G^A(E,V)], \quad (1)$$

where $G^{A/B}$ represent the retarded and advanced Green functions of the scattering region and $\Gamma_{L/R}$ are the coupling functions from the left and right electrodes. The current is calculated by integrating the transmission function over the energy bias window by the following formula:

$$I(V) = \frac{2e}{h}\int_{\mu_L}^{\mu_R} T(E,V)[f(E-\mu_L) - f(E-\mu_R)]dE, \quad (2)$$

where $f(E-\mu_{L/R})$ are the Fermi distribution functions of electrons in the electrodes. $\mu_L = E_f + eV/2$ and $\mu_R = E_f - eV/2$ are the chemical potentials of the left and right electrodes, with E_f the Fermi energy at zero bias.

3 Results and Discussion

3.1 I-V curve & transmission

For both the unreconstructed and reconstructed configurations, the current as a function of bias is shown in Figure 2. Two features can be clearly observed. First, at low bias($\leq$ 0.3V), the current in the reconstructed case is much larger than that in the unreconstructed one(see Figure 2a). For example, at V=0.2V, the current in the reconstructed case is 11.08 μA, in contrast to that (7.02 μA) in the unreconstructed case; the ratio of them is as high as 158%. Apparently, surface reconstruction greatly enhances the current in these devices. Second, with the further increase of the bias, the difference finally becomes very small. As the current is the transmission function dependence over the energy bias window, the behavior of the transmission functions at zero bias will provide the understanding on the origins of the above characteristics presented in the I-V curves, which will be analyzed in the following.

The transmission spectra are given in Figure 3. It is seen that in both the unreconstructed and reconstructed cases, the transmission peaks mediated by the highest occupied molecular orbitals (HOMO) and the lowest unoccupied molecular orbitals (LUMO) of the C_{60}s are clearly observed. The HOMO peaks are located around -1.0 eV, while the LUMO peaks are located close to the Fermi level in both cases. Between these transmission peaks, there is a transmission gap about 0.5 eV. The LUMO mediated transmission peak of C_{60}s around the Fermi level is consistent with all other studies in the literature.[5,31,47] However, big differences are also found in the two cases. The most important two differences lie in the height and the position of the LUMO peaks. The LUMO transmission peak (with height $\sim$1.5) in the unreconstructed case is much higher than that (with height $\sim$0.9) in the reconstructed case, but the peak position ($\sim$ 0.1 eV) in the reconstructed case is much closer to the Fermi level than that ($\sim$ 0.4 eV) in the reconstructed case. Besides the change of shape and peak height, the overall transmission function in the reconstructed case is shifted to lower energy relative to the unreconstructed case. Especially, although the LUMO peak in the unreconstructed case is much higher than the reconstructed one, at around the Fermi level the transmission coefficient is much larger in the reconstructed case. Specifically, the equilibrium conductance (0.87 G_0) in the reconstructed case is much larger than that (0.49 G_0) in the unreconstructed one. This explains why the current at low bias in the reconstructed case is much larger. Another point to note is that, although the reconstruction lowers the height of the LUMO peak, it greatly enhances the transmission in the HOMO-LUMO gap. In clear contrast, in this gap, the transmission in the unreconstructed case is almost zero.

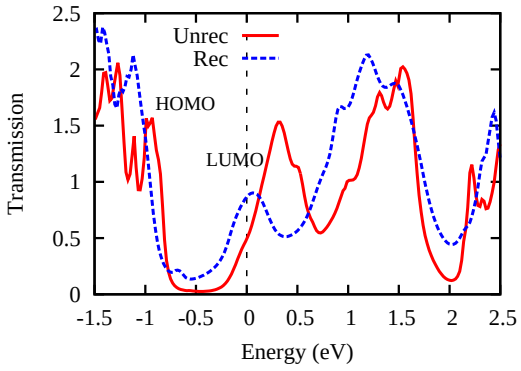

Fig. 3 (color online) Transmission spectra of the unreconstructed and reconstructed cases.

3.2 PDOS & MO-PDOS

In order to understand the differences in the transmission function, the projected density of states (PDOS) of the whole C_{60}s has been analyzed. By comparing the PDOS in Figure 4 and the transmission in Figure 3, we find that the PDOS follows exactly the same trend in the transmission, namely, the LUMO peak in the PDOS of the reconstructed case is much more broadened, much lower and much closer to the Fermi level. Meanwhile, the PDOS in the HOMO-LUMO gap is much larger in the reconstructed structure. These characteristics of course arise from the differences in the electrode-molecule interface structures and the local bonding features. In the unreconstructed case, the C_{60} molecule just sits with a hexagon at the *hcp* hollow site of the Cu(111) surface, thus only 3 bonds are formed between the molecule and the electrode surface. However, in the reconstructed case, besides the 3 bonds formed between the bottom hexagon of the molecule and the *fcc* hollow site of the first complete atomic layer of the Cu(111) surface, there are other 9 C-Cu bonds formed between the C_{60} molecule and the layer with missing atoms (see Figure 1b).[48] Thus, the electrode-molecule coupling in the reconstructed case is much stronger and it leads to many different consequences indicated above.

It is well known that, when a metal is deposited onto a semiconductor, the wave function of an electron in the semiconductor must match that of an electron in the metal at the metal-semiconductor interface. Since the Fermi levels of the two materials must match at the interface, gap states will be formed and decay deep into the semiconductor.[49] The Cu(111)-C_{60} interface is effectively just such a metal-semiconductor system and gap states are naturally formed. These gap states arise from the hybridization between the Cu(111) surface and the C_{60}s and thus the strength of the coupling between them directly determines the magnitudes of the gap states. In order to see how the molecular orbitals are changed and how they contribute to the gap states, we have projected the total density of states onto the molecular orbitals(MO-PDOS) in a surface adsorption system which contains five Cu(111) atomic layers and a C_{60} monolayer. To see the change of the molecular orbitals, for comparison, we have also considered a hypothetical system which excludes the Cu(111) atomic layers and keeps the coordinates of the C atoms exactly the same as those in the fully relaxed Cu(111)-C_{60} system. The total density of states of the monolayer are also projected onto the individual molecular orbitals.

In the hypothetical system, we see that the PDOS of each molecular orbital still consists of an isolated peak(see Figures 5a and 5b). However, in the Cu(111)-C_{60} system, the contribution of each molecular orbital consists of a main peak and many secondary peaks in a very large energy range(see Figures 5c and 5d). In both the reconstructed and the unrecon-

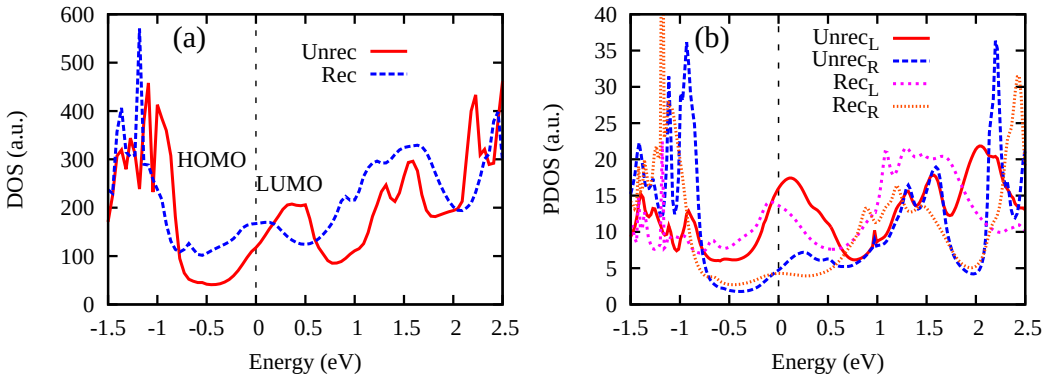

Fig. 4 (color online) Density of states projected on C_{60}s in the transport calculations: (a) Total DOS on C_{60}s; (b) The PDOS of selected subgroups of C atoms. The subscript "L" means the leftmost 6 C atoms which are closest to the left electrode and "R" means the rightmost 6 C atoms of the left C_{60} molecule which lie at the C_{60}-C_{60} interface.

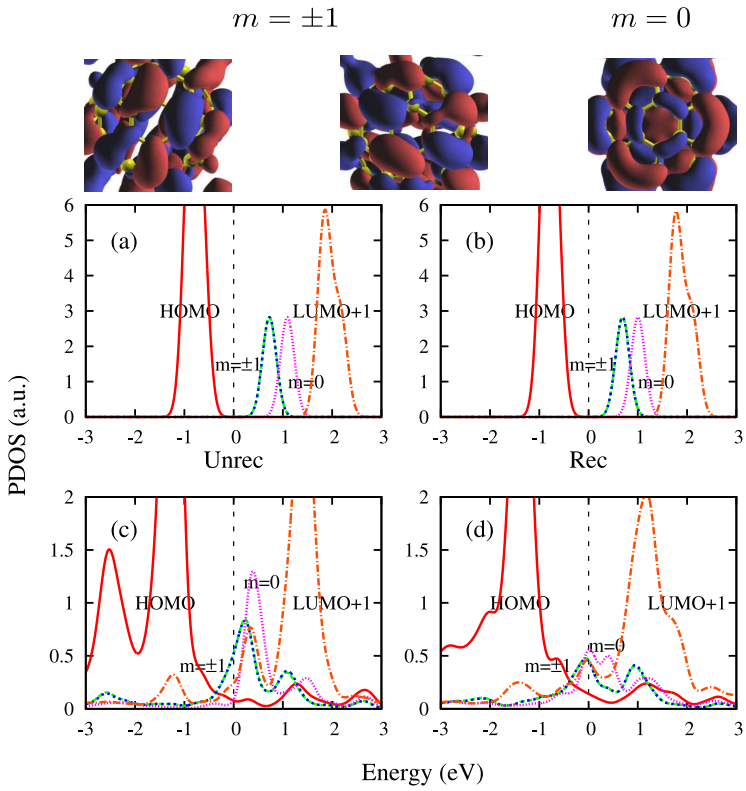

Fig. 5 (color online) Density of states of C_{60} projected on different molecular orbitals for: (a) the unreconstructed structure with the Cu(111) substrate excluded; (b) the reconstructed structure with the Cu(111) substrate excluded; (c) the unreconstructed Cu(111)-C_{60} system; (d) the reconstructed Cu(111)-C_{60} system. Since we focus on the LUMOs, only the three LUMO orbitals are given separately while the HOMO orbitals and LUMO+1 orbitals are added together, respectively. In addition, the wave functions of the three LUMO orbitals, labelled by $m = -1, 0, +1$, are plotted at the top of the figure. It is obvious that the $m = 0$ orbital is threefold rotationally symmetrical with respect to the z axis while $m = -1$ and $m = +1$ are not, which gives rise to the fact that the energy of $m = 0$ orbital is different from $m = -1$ and $m = +1$.

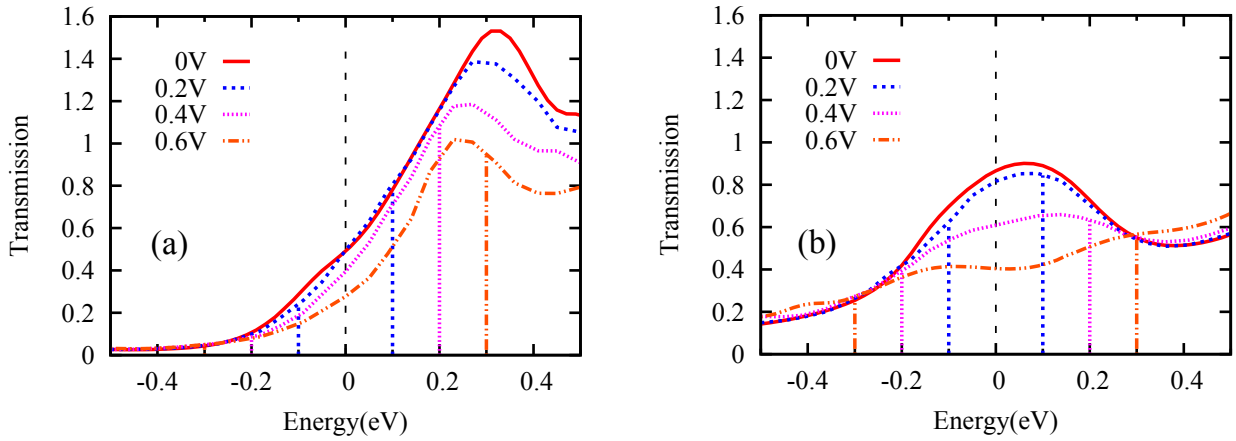

Fig. 6 (color online) The evolution of transmission spectra with an increase of finite bias: (a) for the unreconstructed case and (b) for the reconstructed case. The two vertical lines with the same color indicate the bias windows.

structed cases, although there may be some differences in the coordinates of the C atoms, the two hypothetical systems give almost the same orbital projected density of states. If we focus on the LUMOs, we see that the threefold degenerate LUMOs are split into two groups. The first group contains two degenerate orbitals labeled by $m = \pm 1$ with lower energy and the second group contains one orbital labeled by $m = 0$ which is higher in energy. The heights of the three peaks with $m = -1$, 0 and +1 are the same. When the monolayer are "deposited" onto the Cu(111) substrate, the main peaks of $m = \pm 1$ orbitals become much lower than the $m = 0$ orbital in the unreconstructed case and their contributions extend to a very large energy range. Such changes in the MO-PDOS from an isolated peak to a main peak accompanied by many secondary peaks arise from the hybridization between the electrode and the C_{60} molecule and are the origin of the gap states. In this case, the contributions of all the three main peaks add up to a high and sharp peak, thus a high transmission peak is observed. However, in the reconstructed case, due to the stronger coupling at the electrode-molecule interface, the contribution of all the three LUMO orbitals decreases further from the main peak and increases to other energy region. Especially, the main peak of the $m = 0$ orbital further splits into double peaks(see Figure 5(d)), which greatly decreases the height of the $m = 0$ orbital. The sum of the $m = -1$, 0 and +1 at the main peak position is much smaller than the unreconstructed case, which results in a much lower LUMO transmission peak.

Besides the height of the transmission peak, the electrode-molecule coupling also affects the charge transfer between the electrode and the molecule. Mulliken population analysis shows that charge transfer of 2.0 electrons from the electrodes to the two C_{60} molecules occurs in the unreconstructed configuration. In comparison, the charge transfer in the reconstructed case is 5.5 electrons. Thus the average excess charge per C_{60} is about 1.0 and 2.8 electrons respectively, which is in good agreement with the literatures,[50] where it is proposed that a C_{60} generally obtains $1 \sim 3$ electrons from the electrodes. Consequently, it is easy to understand why the LUMO-mediated transmission peak position of the reconstructed case is shifted to lower energy relative to the other case since the larger charge transfer fills more states and thus pushes the Fermi level to higher energy. Eventually, the Fermi level lies almost in the middle of the LUMO peak in the reconstructed case, while it lies at the lower edge in the unreconstructed case (see Figure 3). Consequently, around the Fermi level, the transmission in the reconstructed case is much larger than the unreconstructed case.

3.3 Further Discussions

In the following, we take an insight into why in the HOMO-LUMO gap it exhibits a considerable density of states from the C_{60} while the transmission is almost zero in the unreconstructed case (see Figure 4a and Figure 3). We extract the PDOS for each C atom and observe the difference in the PDOS between the C atoms close to the electrodes and those at the C_{60}-C_{60} interface. It is obvious that, the PDOS in the HOMO-LUMO gap is mainly contributed by the C atoms close to the electrodes and the contributions at the C_{60}-C_{60} interface is negligible. From Figure 4b, we find that PDOS in the HOMO-LUMO gap (the gap states) decay rapidly to the center of the two C_{60} monolayers. Due to the greatly suppressed density of states in the HOMO-LUMO gap at the C_{60}-C_{60} interface, it effectively acts as a potential barrier, thus the electron transmission is greatly blocked.[47] In contrast, in the reconstructed case, stronger coupling between the C_{60}s and the electrodes

increases the PDOS of C atoms at the C_{60}-C_{60} interface(see Figure 5b) and thus enhances the electron transmission in the HOMO-LUMO gap (see Figure 3).

Next, we turn to see the origin why the difference between the currents in the two cases becomes gradually smaller and finally neglectable at higher bias (with $V \geq 0.6$ V). We have gathered the transmission functions at different biases together(see Figure 6). It is seen that, due to the relative shift of the LUMOs of two C_{60} monolayers with the increase of the bias and thus the decrease of the coupling between them, the heights of the LUMO peaks in the transmission functions of both the reconstructed and unreconstructed cases decrease very fast. Since at higher bias, in the reconstructed case, the LUMO peak becomes lower and flatter, the current increases much slower. In contrast, in the unreconstructed case, the main part of the LUMO peak enters the bias windows, thus the current increases quickly and the difference between the two cases becomes rapidly small.

Finally, for molecule-molecule interacting systems, the van der Waals (vdW) interaction should be generally taken into consideration. However, we want to point out that, the vdW interaction between the C_{60} molecules and in the adsorption on electrodes has been neglected due to the following reasons: First, LDA is already able to produce an accurate C_{60}-C_{60} distance. The error is less than 1% in bulk C_{60} compared with the experimental value.[51] Our structures are also ralaxed by taking the experimental value as the initial distance using LDA. At the C_{60}-Cu interface, the chemical bonds are much stronger than the vdW interaction. Thus, from geometry, the neglect of the vdW interaction is reasonable. Second, it is well known that the vdW interaction mainly changes the molecule-molecule distance. It has very little effects on the electronic structure. Therefore, in the electron transport calculations, the correction of vdW interaction can also be safely neglected.

4 Conclusion

In summary, by combining density functional theory with the nonequilibrium Green's function, we have investigated the electronic structures and transport properties of C_{60}s on Cu(111) with reconstructed and unreconstructed surfaces. Due to the formation of the 7-atom vacancy in the Cu(111) surface, the coupling and hybridization between the metallic electrodes and the C_{60} molecule is greatly strengthened, which results in many consequences, such as lower LUMO DOS peak, more PDOS contribution to the transmission in the HOMO-LUMO gap and more charge transfer from the electrodes to C_{60} molecule. Although the LUMO transmission peak decreases greatly, the Fermi level almost shifts to the center of this transmission peak. Thus the transmission around the Fermi level in the reconstructed case is much larger than the unreconstructed one. These changes directly lead to the great enhancement of the current at low bias. The equilibrium conductance is increased from 0.49 G_0 to 0.87 G_0 and the current at low bias is increased by more than 50% due to the surface reconstruction. Consequently, the metal surface reconstruction plays a very important role in the electronic structures and transport properties of two-terminal molecular junctions. In the simulation and design of molecular devices, especially when it is expected to reproduce computationally the experimental observations, it is crucial to take the contact details (such as surface reconstruction, adatoms on metallic surface[52] and so on) into full consideration.

ACKNOWLEDGEMENT

This work is supported by the National Science Foundation of China under Grant Nos. 11104272, 11174289 and 11334003, Hefei Center for Physical Science and Technology under Grant no. 2012FXZY004 and Director Grants of CASHIPS. The calculations were performed in Center for Computational Science of CASHIPS, the ScGrid of Supercomputing Center and Computer Net work Information Center of Chinese Academy of Science.

References

1 N. Kobayashi, M. Brandbyge and M. Tsukada, *Physical Review B*, 2000, **62**, 8430.
2 Amar H. Flood, J. Fraser Stoddart, David W. Steuerman and James R. Heath, *Science*, 2004, **306**, 2055.
3 N. J. Tao, *Nature nanotechnology*, 2006, **1**, 173.
4 V. M. García-Suárez and C. J. Lambert, *Nanotechnology*, 2008, **19**, 455203.
5 X. H. Zheng, W. C. Lu, T. A. Abtew, V. Meunier and J. Bernholc, *ACS Nano*, 2010, **4**, 7205.
6 B. W. Heinrich, M. V. Rastei, D.-J. Choi, T. Frederiksen and L. Limot, *Physical Review Letters*, 2011, **107**, 246801.
7 A. S. Martin, J. R. Sambles and G. J. Ashwell, *Phys. Rev. Lett.*, 1993, **70**, 218.
8 J. K. Gimzewski and C. Joachim, *Science*, 1999, **283**, 1683.
9 P. Zhao, D. S. Liu and G. Chen, *Journal of Chemical Physics*, 2013, **139**, 084318.
10 J. Lan, X. H. Zheng, H. Hao, X. L. Wang, X. Q. Shi and Z. Zeng, *Journal of Applied Physics*, 2014, **115**, 013702.
11 I.-H. Chu, J. Trinastic, L.-W. Wang and H.-P. Cheng, *Physical Review B*, 2014, **89**, 115415.
12 Y.-W. Son, M. L. Cohen and S. G. Louie, *Nature*, 2006, **444**, 347.
13 J. Bai, R. Cheng, F. Xiu, L. Liao, M. Wang, A. Shailos, K. L. Wang, Y. Huang and X. Duan, *Nature Nanotechnology*, 2010, **5**, 655.
14 R. H. M. Smit, Y. Noat, C. Untiedt, N. D. Lang, M. C. van Hemert and J. M. van Ruitenbeek, *Nature*, 2002, **419**, 906.
15 K. W. Hipps, *Science*, 2001, **294**, 536.
16 A. Nitzan and M. A. Ratner, *Science*, 2003, **300**, 1384.
17 R. Berndt, J. Kröger, N. Néel and G. Schull, *Physical Chemistry Chemical Physics*, 2010, **12**, 1022.
18 N. Hauptmann, F. Mohn, L. Gross, G. Meyer, T. Frederiksen and R. Berndt, *New Journal of Physics*, 2012, **14**, 073032.

19 S. Bilan, L. a. Zotti, F. Pauly and J. C. Cuevas, *Physical Review B*, 2012, **85**, 205403.

20 W. Hong, D. Z. Manrique, P. Moreno-García, M. Gulcur, A. Mishchenko, C. J. Lambert, M. R. Bryce and T. Wandlowski, *Journal of the American Chemical Society*, 2012, **134**, 2292.

21 E. Leary, M. T. González, C. van der Pol, M. R. Bryce, S. Filippone, N. Martín, G. Rubio-Bollinger and N. Agraït, *Nano Letters*, 2011, **11**, 2236.

22 T. Markussen, M. Settnes and K. S. Thygesen, *Journal of Chemical Physics*, 2011, **135**, 144104.

23 Guillaume Schull, Yannick J. Dappe, César González, Hervé Bulou and Richard Berndt, *Nano Letters*, 2011, **11**, 3142.

24 G. Schull, T. Frederiksen, A. Arnau, D. Sánchez-Portal and R. Berndt, *Nature Nanotechnology*, 2011, **6**, 23.

25 L.-L. Wang and H.-P. Cheng, *Physical Review B*, 2004, **69**, 045404.

26 W. Pai, C.-L. Hsu, M. Lin, K. Lin and T. Tang, *Physical Review B*, 2004, **69**, 125405.

27 W. W. Pai, H. T. Jeng, C.-M. Cheng, C.-H. Lin, X. Xiao, A. Zhao, X. Zhang, G. Xu, X. Q. Shi, M. A. Van Hove, C.-S. Hsue and K.-D. Tsuei, *Physical Review Letters*, 2010, **104**, 036103.

28 L. Tang, X. Zhang, Q. Guo, Y.-N. Wu, L.-L. Wang and H.-P. Cheng, *Physical Review B*, 2010, **82**, 125414.

29 J. Lu, P. S. E. Yeo, C. K. Gan, P. Wu and K. P. Loh, *Nature nanotechnology*, 2011, **6**, 247.

30 X.-Q. Shi, M. A. Van Hove and R.-Q. Zhang, *Physical Review B*, 2012, **85**, 075421.

31 J. Taylor, H. Guo and J. Wang, *Physical Review B*, 2001, **63**, 121104.

32 T. Ono and K. Hirose, *Physical Review Letters*, 2007, **98**, 026804.

33 C. Evangeli, K. Gillemot, E. Leary, M. T. González, G. Rubio-Bollinger, C. J. Lambert and N. Agraït, *Nano Letters*, 2013, **13**, 2141.

34 B. C. Hsu, C.-Y. Lin, Y.-S. Hsieh and Y.-C. Chen, *Applied Physics Letters*, 2012, **101**, 243103.

35 H. I. Li, K. Pussi, K. J. Hanna, L.-L. Wang, D. D. Johnson, H.-P. Cheng, H. Shin, S. Curtarolo, W. Moritz, J. A. Smerdon, R. McGrath and R. D. Diehl, *Phys. Rev. Lett.*, 2009, **103**, 056101.

36 X.-Q. Shi, M. A. Van Hove and R.-Q. Zhang, *Phys. Rev. B*, 2012, **85**, 075421.

37 G. Otero, C. Gonzalez, A. L. Pinardi *et al.*, *Phys. Rev. Lett.*, 2010, **105**, 216102.

38 P. Maksymovych, D. C. Sorescu, O. Voznyy and J. T. Yates Jr, *Journal of the American Chemical Society*, 2013, **135**, 4922–4925.

39 X. Zheng, J. Lan, X. Wang, L. Huang, H. Hao and Z. Zeng, *Applied Physics Letters*, 2012, **101**, 053101.

40 G. Kresse and J. Furthmuller, *Physical Review B*, 1996, **54**, 11169.

41 G. Kresse and D. Joubert, *Physical Review B*, 1999, **59**, 1758.

42 J. M. Soler, E. Artacho, J. D. Gale, A. Garcia, J. Junquera, P. Ordejon and D. Sanchez-Portal, *J. Phys.: Condens. Matter*, 2002, **14**, 2745.

43 M. Brandbyge, J.-L. Mozos, P. Ordejón, J. Taylor and K. Stokbro, *Phys. Rev. B*, 2002, **65**, 165401.

44 X. H. Zheng, J. Lan, H. Hao and Z. Zeng, *E-Science Technology and Application*, 2013, **4**, 90.

45 S. Datta, *Electronic Transport in Mesoscopic Systems*, Cambridge University Press, Cambridge, England, 1995.

46 H. Haug and A.-P. Jauho, *Quantum Kinetics in Transport and Optics of Semiconductors*, Springer, Berlin, 1996.

47 X. H. Zheng, X. L. Wang, Z. X. Dai and Z. Zeng, *Journal of Chemical Physics*, 2011, **134**, 044708.

48 X.-Q. Shi, M. A. Van Hove and R.-Q. Zhang, *J. Mater. Sci.*, 2012, **47**, 7341.

49 M. Sogo, Y. Sakamoto, M. Aoki, S. Masuda, S. Yanagisawa and Y. Morikawa, *J. Phys. Chem. C*, 2010, **114**, 3504.

50 K.-D. Tsuei, J.-Y. Yuh, C.-T. Tzeng, R.-Y. Chu, S.-C. Chung and K.-L. Tsang, *Phys. Rev. B*, 1997, **56**, 15412.

51 K.-P. Bohnen and R. Heid, *Physical review letters*, 1999, **83**, 1167.

52 T. Frederiksen, G. Foti, F. Scheurer, V. Speisser and G. Schull, *Nature Communications*, 2014, **5**, 1.

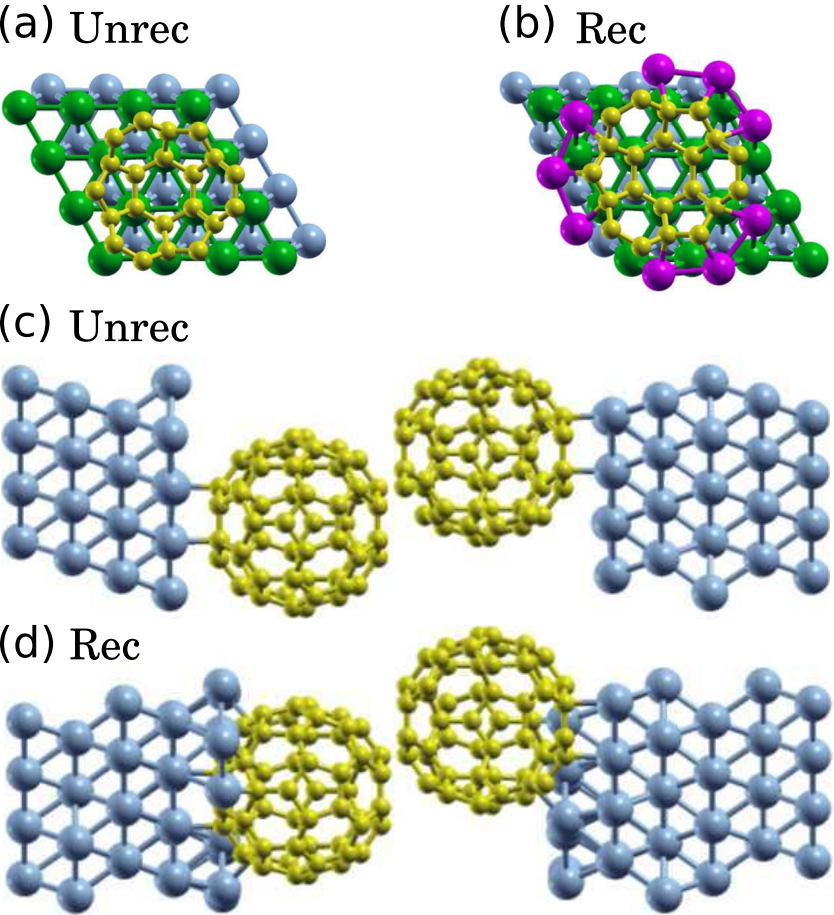

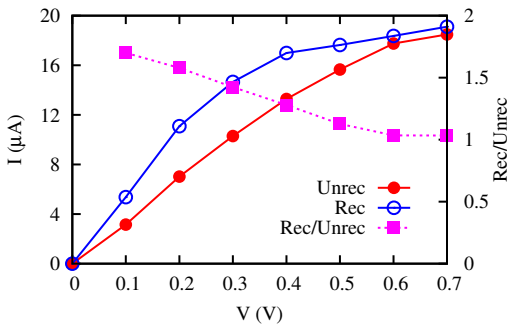

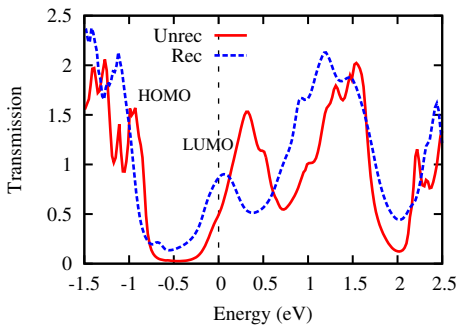

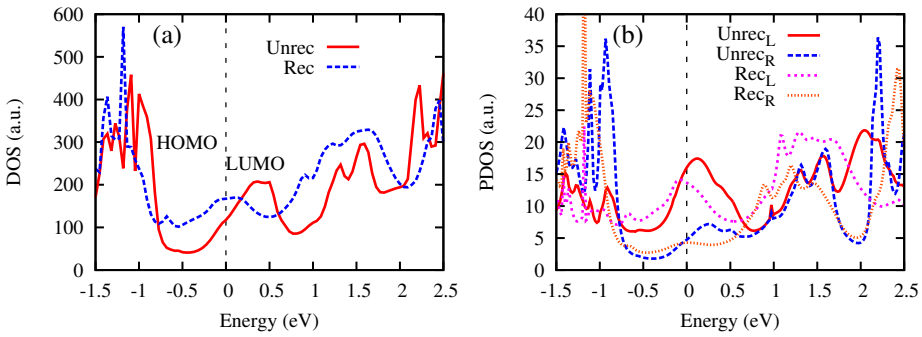

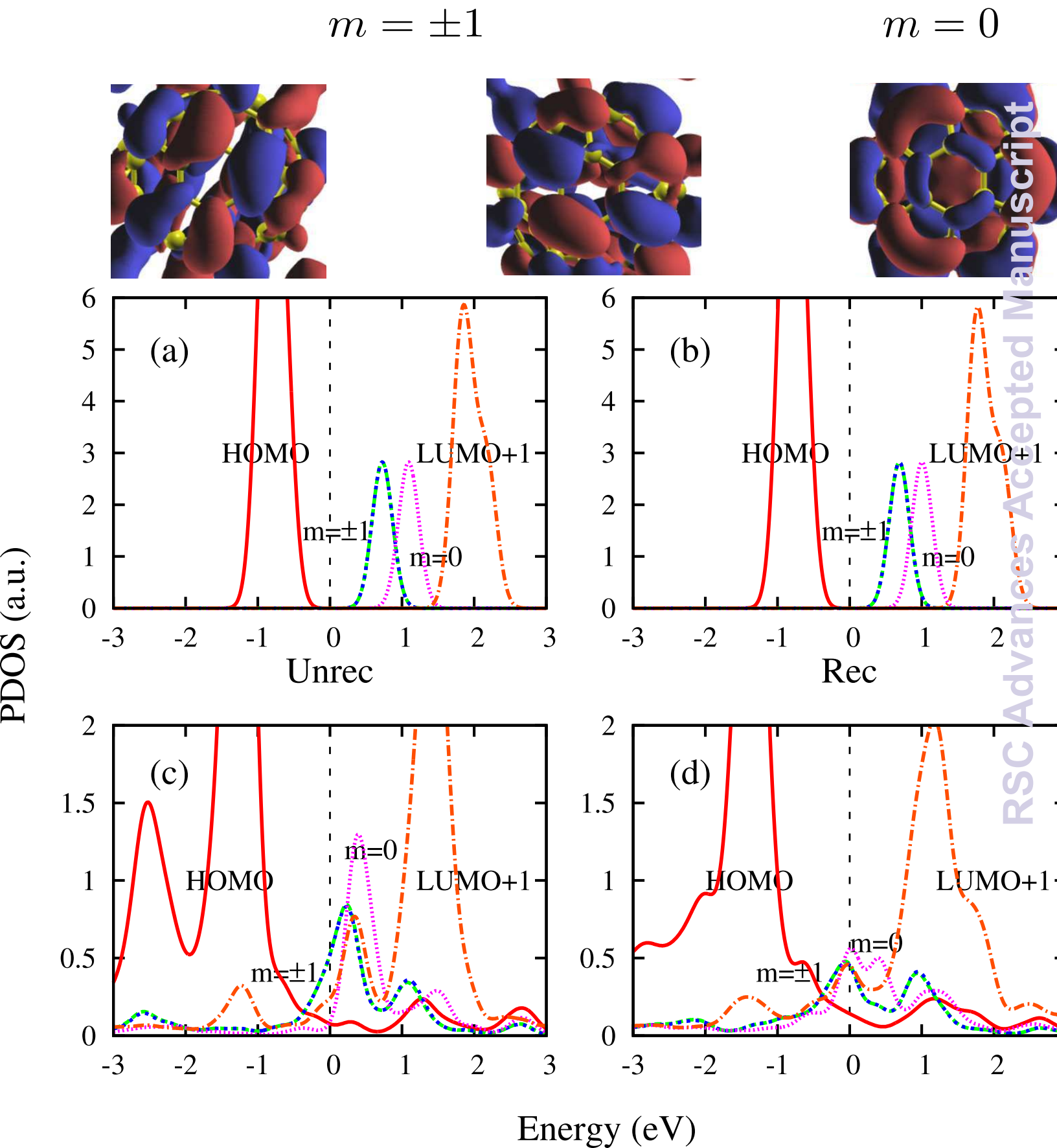

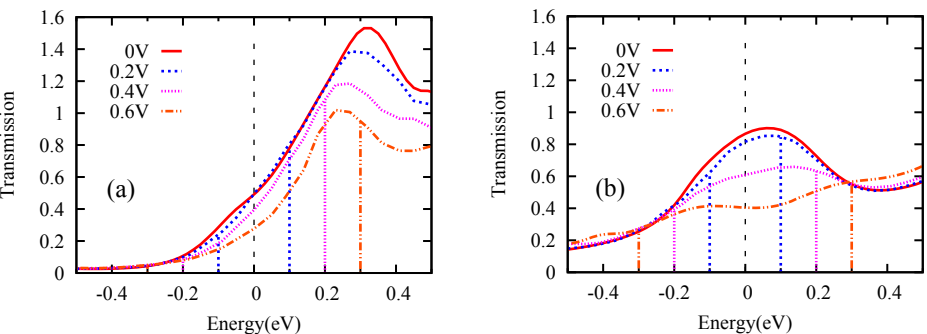

At the C60/Cu(111) interface, electrode surface reconstruction (Rec) increases electrical current compared to that for the unreconstructed (Unrec) surface.